



## Effects on Chilean Vertical Reference Frame due to the Maule Earthquake co-seismic and post-seismic effects



Henry D. Montecino<sup>a,b</sup>, Silvio R.C. de Freitas<sup>a</sup>, Juan C. Báez<sup>c</sup>, Vagner G. Ferreira<sup>d,\*</sup>

<sup>a</sup> Geodetic Sciences Graduation Course, Federal University of Paraná, Curitiba, Brazil

<sup>b</sup> Department of Geodesy Science and Geomatics, University of Concepción, Los Angeles, Chile

<sup>c</sup> National Seismological Center, University of Chile, Santiago, Chile

<sup>d</sup> School of Earth Sciences and Engineering, Hohai University, Nanjing, China

### ARTICLE INFO

#### Keywords:

Chilean vertical datum  
GRACE  
GNSS  
Deformations  
Maule Earthquake

### ABSTRACT

The Maule Earthquake ( $M_w = 8.8$ ) of February 27, 2010 is among the strongest earthquakes that occurred in recent years throughout the world. The crustal deformation caused by this earthquake has been widely studied using GNSS, InSAR and gravity observations. However, there is currently no estimation of the possible vertical deformations produced by co-seismic and post-seismic effects in segments of the Chilean Vertical Reference Frame (CHVRF). In this paper, we present an estimation of co-seismic and post-seismic deformations on the CHVRF using an indirect approach based on GNSS and Gravity Recovery and Climate Experiment (GRACE) data as well as by applying a trajectory model. GNSS time series were used from 10 continuous GNSS stations in the period from 2007 to 2015, as well as 28 GNSS temporary stations realized before and after the earthquake, and 34 vertical deformation vectors in the region most affected by the earthquake. We considered a set of 147 monthly solutions of spherical harmonic gravity field that were expanded up to degree, as well as order 96 of the GRACE mission provided by Center for Space Research, University of Texas at Austin (UT-CSR) process center. The magnitude of vertical deformation was estimated in part of the Chilean vertical network due to the co-seismic and post-seismic effects. Once we evaluated the hydrological effect, natural and artificial jumps, and the effect of glacial isostatic adjustment in GNSS and GRACE time series, the maximum values associated to co- and post-seismic deformations on orthometric height were found to be  $\sim -34$  cm and 5 cm, respectively. Overall, the deformation caused by the Maule earthquake in orthometric heights is almost entirely explained by the variation in the ellipsoidal heights (over 85% in co-seismic jump); however, coseismic jump in the geoid reached  $-3.3$  mm, and could influence the maintenance of a modern vertical reference network in a medium to long term. We evaluated the consistency for a segment of the CHVRF after the earthquake and recommended precautions for using the CHVRF in the region.

### 1. Introduction

Three of the fundamental objectives of Geodesy are the definition (System), realization (Frame) and maintenance of the International Height Reference System (IHRF), which is consistent with Theme 1 of the Global Geodetic Observing System (GGOS) project (Ihde et al., 2015). The goal of establishing the IHRF is to remove inconsistencies among heights in the geometric and in the Earth's potential field spaces. Consistent height information will eliminate complications in civil constructions around the world that link data from different height zones, and will facilitate interpretation of sea level records at globally distributed tide gauges. However, several geodynamic aspects must be considered when establishing and maintaining the Vertical Reference

Frame.

For instance, the quantification and modeling of geodynamic effects are fundamental for the precise determination of heights of points and their trajectory in time, which allow a correct interpretation of these phenomena. One important aspect is linked to co-seismic and post-seismic deformations, associated with large earthquakes. Recent discussions have been based on the modern tools of Geodesy (Sun, 2014), which analyze the geometric space (Du et al., 2013) or the geopotential space (Li and Shen, 2012), but do not provide a link between the two spaces. However, this link is fundamental for understanding the implications of co-seismic and post-seismic effects on vertical reference surfaces and associated frames.

The Maule Earthquake ( $M_w = 8.8$ ) event in February of 2010 is one

\* Corresponding author at: School of Earth Sciences and Engineering, Hohai University, Nanjing, China.

E-mail addresses: [henrymontecino@udec.cl](mailto:henrymontecino@udec.cl) (H.D. Montecino), [sfreatas@ufpr.br](mailto:sfreatas@ufpr.br) (S.R.C. de Freitas), [jcbaz@csn.uchile.cl](mailto:jcbaz@csn.uchile.cl) (J.C. Báez), [vagnergf@hhu.edu.cn](mailto:vagnergf@hhu.edu.cn) (V.G. Ferreira).

of the largest seismic events that has occurred in recent years in South America. To date, more than 200 scientific publications are available in the field of Geodesy, Geophysics, and Geology related to the Maule Earthquake, most of which are based on different types of geodetic observations (e.g., GNSS, InSAR, and satellite gravimetry). For reference, we emphasize the following studies: an estimation of the distribution of co-seismic and post-seismic slip to assess the spatial variability of frictional properties on the south-central Chilean megathrust (Lin et al., 2013); the convergence of the Nazca and South American plates reported by Moreno et al. (2011); the magnitude and distribution of the slip effect quantified by Pollitz et al. (2011); co-seismic gravity change observation via satellite gravimetry presented in Heki and Matsuo (2010); and discussion on the behavior of short and long term changes in gravity produced by the Maule Earthquake by Tanaka and Heki (2014).

Rivas (2010) furthered the studies of Maule Earthquake and presented its implications on the official cartography of Chile. More recently, Sánchez and Drewes (2015) presented an estimation of post-seismic horizontal deformation based on the least squares collocation. However, most of the studies related to this event refer only to the geometrical aspects in the context of the Earth's crust deformations. However, there are no studies available to date on the implications of the co-seismic and post-seismic vertical deformations of the Maule Earthquake regarding the maintenance and evolution of the Chilean Vertical Reference Frame (CHVRF) and the long changes of the geoid in the region.

Thus, in this contribution, we present an estimate of deformation in part of the CHVRF generated by co-seismic and post-seismic effects associated with the Maule Earthquake based on the integration of GNSS and GRACE observations, taking the contribution of the hydrological effect and Glacial Isostatic Adjustment (GIA) into account as well as considering a trajectory model c.f. Bevis and Brown (2014).

An indirect alternative estimate the orthometric heights, disregarding the deflection of the vertical, is through the relation (Hofmann-Wellenhof and Moritz, 2005):

$$H = h - N, \quad (1)$$

where  $H$ ,  $h$  and  $N$  are the orthometric, ellipsoidal, and geoid heights, respectively. Linear trends of those quantities may be expressed as:

$$\dot{H} = \dot{h} - \dot{N}, \quad (2)$$

where  $\dot{H}$ ,  $\dot{h}$  and  $\dot{N}$  are the linear trends in orthometric, ellipsoidal, and geoid heights, respectively. Here, it is proposed that the orthometric height at any epoch ( $t$ ) can be expressed more rigorously as:

$$\begin{aligned} H(t) &\cong H(t_0) + \dot{H}(t - t_0) + \sum_{k=1}^{nf} H(t)_{osc_k} + \sum_{j=1}^{nj} H(t)_{jump_j} \\ &\quad + \sum_{i=1}^{nT} H(t)_{trans_i} \\ H(t) &\cong \left( h(t_0) + \dot{h}(t - t_0) + \sum_{k=1}^{nf} h(t)_{osc_k} + \sum_{j=1}^{nj} h(t)_{jump_j} \right. \\ &\quad \left. + \sum_{i=1}^{nT} h(t)_{trans_i} \right) \dots \\ &\quad - \left( N(t_0) + \dot{N}(t - t_0) + \sum_{k=1}^{nf} N(t)_{osc_k} + \sum_{j=1}^{nj} N(t)_{jump_j} + \sum_{i=1}^{nT} N(t)_{trans_i} \right) \end{aligned} \quad (3)$$

where  $t_0$  is the epoch of definition, the dot over the respective heights represent the linear trends, the subscript "osc<sub>k</sub>", "jump<sub>j</sub>" and "trans<sub>i</sub>" are the amplitude of  $k = 1, \dots, nf$  periodic components (e.g., annual and semi-annual hydrologic effects), possible  $j = 1, \dots, nj$  jumps associated with natural or instrumental effects (e.g. co-seismic effect; change of GNSS antenna), and post-seismic deformation term for  $i = 1, \dots, nT$ ,

respectively.

Previous studies in North America have considered the changes in the geoid heights, but only by quantifying their linear temporal variations (see, e.g., Rangelova et al., 2012, 2010). For instance, Jacob et al. (2012) quantified the impact of hydrologic effects, earthquakes, volcanic, and the post-glacial uplift effect on the geoid, noting the importance of considering these effects for the implementation of a dynamic geoid in North America. Furthermore, Panet et al. (2007) and De Linage et al. (2009) have also attempted to separate the gravimetric signal from co- and post-seismic effects associated with the 2004 Sumatra-Andaman earthquake using GRACE observations, and modeling the co-seismic effect by using normal modes summation. Conversely, trajectory models for modelling the surface crust deformations have been developed, which are generally based on GNSS time series data. However, none of these studies have analyzed the variations of the geoid and ellipsoidal height using an integrated approach.

Thus, in this contribution, we estimated the changes in part of the CHVRF generated by co-seismic and post-seismic effects associated with the Maule Earthquake based on the integration of GNSS and GRACE observations. To do so, we have considered the contribution of the hydrological effects and Glacial Isostatic Adjustment (GIA) on the monthly geoid changes derived from GRACE measurements. Finally, a trajectory model as proposed by Bevis and Brown (2014) was considered in order to parameterize accelerating patterns of displacement, specifically, the post-seismic transient deformation in coordinate time-series.

## 2. The Maule Earthquake and the CHVRF

It is of special importance in Chile to control crustal dynamic phenomena and its implication on several scientific and practical applications. In this context, it is mandatory to modelling the deformation on the CHVRF due to the co- and post-seismic effects. This is important in order to establish the temporal evolution of the CHVRF for a consistent integration of its segments and its relationship with the regional vertical networks of the neighboring countries as well as the IHRF.

Due to Chile's unique geographic features, such as its size and shape, the CHVRF is measured in seven different segments related to the tide gauges of Arica, Antofagasta, Valparaíso, San Antonio, Talcahuano, Puerto Montt, and Punta Arenas (Maturana and Barriga, 2002). Only a few of these segments were re-measured with the goal of updating the heights of the network after strong earthquakes, for example, the 1960 Valdivia earthquake (Mw9.5), the 1965 La Ligua Earthquake (Mw7.4), and the 1985 Algarrobo Earthquake (Mw8.0) events. However, there has been no recent re-leveling of the segments of the CHVRF near the epicenter of the Maule Earthquake. This is mainly due to the expensive costs of the spirit leveling procedure on a large and involved region. Thus, exploring indirect alternatives for estimating deformations on the CHVRF has become vital.

Although Chile is known to be a highly seismic country, there is no a specific model built aiming to update the positions in the vertical geodetic networks. Nonetheless, there are regional velocity models that are primarily utilized for updating the horizontal components (e.g., east and north coordinates) considering only linear trends. Velocity models have been developed in South America based on GNSS observations through different research projects, such as the Velocity Model for South America and the Caribbean (VEMOS) by Drewes and Heibach (2012) and, more recently, VEMOS2015 proposed by Sánchez and Drewes, (2016). Consequently, there is currently no procedure for modelling the vertical deformations, which is the issue considered in this study.

Since GNSS and geoid time series contain signals of various geophysical phenomena (e.g., hydrological loading, post-glacial uplift, and earthquake deformations), we have considered them in the present study while modelling the deformations in a segment of the CHVRF.

**Table 1**  
GNSS stations used and institutions responsible for the operation.

GNSS Station name	Responsible institution
NIEB, LLFN, LNQM, UDEC, ANTC, VALP and LAJA	Ohio State University (OSU)
PMO1	German Research Centre for Geosciences (GFZ)
CONZ	The Transportable Integrated Geodetic Observatory (TIGO)
SANT	NASA Jet Propulsion Laboratory (JPL)

### 3. Data and methods

We created the strategies for modeling the Maule Earthquake effects on the CHVRF by considering geometric and physical effects. Thought, considering that there is a consensus surrounding the CHVRF as a normal-orthometric height system, Eq. (2) can be used to determine true variations in the network due to the estimated temporal variations of the ellipsoidal and geoid/quasigeoid heights. The linear change of the geometric component ( $h$ ) can be estimated by GNSS surveying obtained via time series provided by institutions and geodetic and geophysical projects. In this study, we used GNSS time series obtained from permanent stations (see Table 1), campaign point positioning (see Fig. 1) in the Maule region before and after the seismic event.

For the physical component ( $\dot{N}$ ), the gravimetric mission Gravity Recovery and Climate Experiment (GRACE) provides temporal variations of the Earth’s gravity field with sufficient precision for the purposes discussed herein, and temporal resolution available weekly and monthly (see, e.g., Bruinsma et al., 2010; Tapley et al., 2004).

### 3.1. Estimation of Earthquake Signature in GNSS-based measurements

GNSS positioning is currently a widely-used technique in geosciences due to its capability in determining coordinates in a global geocentric system, and for providing consistent time series of station positions with accuracy at the millimeter level. It is sufficient for modelling several geodynamic processes. In this study, we used two sets of GNSS stations. The first set included 28 temporary GNSS stations occupied in observing campaigns before and after the Maule earthquake. We used these stations for estimating the co-seismic effects. A second set of permanent GNSS stations (see Table 1) furnished position time series in the period 2007–2015 (see Fig. 1), which allowed us to analyze the co-seismic and post-seismic effects associated with the 2010 Maule Earthquake.

The GNSS data processing was performed with Bernese 5.2 software. We used GPS precise orbits came from International GNSS Service (IGS). We used the Vienna Mapping Function (Boehm et al., 2006) to model the tropospheric refraction, as well as absolute phase center antenna correction (Schmid et al., 2007). Ionosphere delays were removed by ion-free dual frequency combination strategy. The geocentric Cartesian coordinates from the time window of 2007–2014 were transformed to geodetic coordinates ( $\varphi, \lambda, h$ ), and only the ellipsoidal height was used to study the displacements due to co and post-seismic effects. Finally, outliers were removed based on the 3 $\sigma$ -rule.

We also used the vertical co-seismic deformations published by Vigny et al. (2011) in order to supplement our GNSS data source, and to get a better representation of the distribution of co-seismic jumps associated to Maule Earthquake. These complementary solutions came from continuous GNSS stations and survey campaign GNSS data. For continuous stations, the co-seismic jumps were determined as the

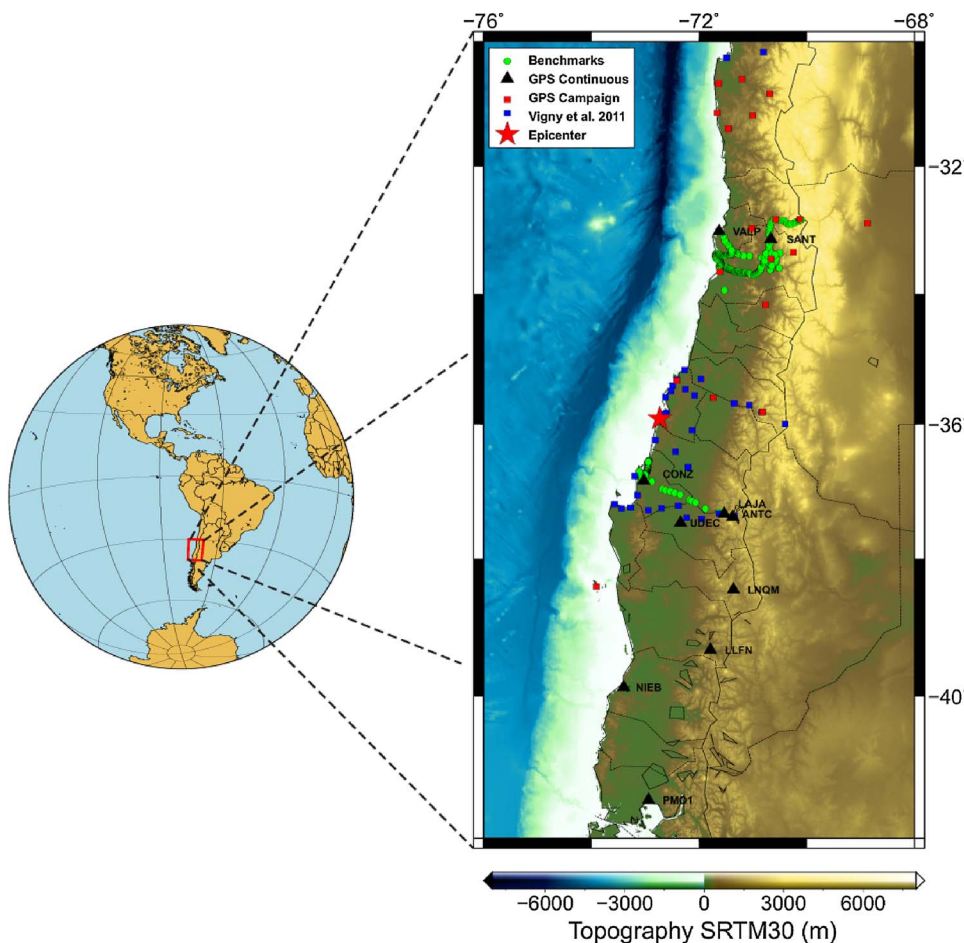


**Fig. 1.** The map of the study region, including topography and bathymetry based on SRTM30 PLUS (Becker et al., 2009). The green, red and blue squares represent the benchmarks of the CHVRF, temporary GNSS stations, and GNSS stations available in Vigny et al. (2011), respectively. The black triangles represent the permanent GNSS stations, and the red star represents the location of the epicenter. (For interpretation of the references to colour in this figure legend, the reader is referred to the web version of this article.)

difference between the day before and the day after the earthquake. For survey sites, we have determined the co-seismic displacements by extrapolating the last known position before the earthquake to the date of the re-survey after the earthquake using the inter-seismic rate, and by comparing the latest to the present positions [for more details, see the supplementary material from Vigny et al., (2011)].

On April 17 of 2011, the IGS changed the Reference System for GPS precise orbits from IGS05 to IGS08. Because we do not have a set of local precise transformation parameters (translation, rotation and scale) necessary to update from IGS05 to IGS08, the effect of the datum change on the heights was considered to be a “jump” within the trajectory model as explained in Sub-section 3.3. In general, we found a systematic average jump of around  $-13$  mm associated with the epoch of datum change. In addition, all earthquakes and GNSS antenna changes occurred during the study period in the stations were modelled through the trajectory model. To identify the epoch of the earthquake and/or an antenna, receiver, or firmware change, we used the catalog published in the US Geological Survey’s website.

Furthermore, we also considered the most important shallow earthquakes in the region besides the Maule Earthquake that occurred between January 2010 and May 2012 (see Fig. 2). The effects of five considered earthquakes on the continuous GNSS time series have values of approximately  $\pm 10$  mm (see Fig. 2).

### 3.2. GRACE-based monthly gravity field solutions

GRACE monthly solutions from August 2002 to March 2016 were used in the analysis linked to the geopotential space. We used data corresponding to 147 monthly solutions of spherical harmonic coefficients (Level 2 products) Release 05 (RL05), developed up to degree and order (d/o) 96. These monthly solutions are based on a set of spherical harmonic coefficients provided by the Center for Space Research, at The University of Texas at Austin (UT-CSR), and are freely available at <ftp://podaac-ftp.jpl.nasa.gov/allData/> (Bettadpur, 2012). The particular choice of the UT-CSR solutions was made because they showed more accuracy relatively to other GRACE process centers (i.e., GFZ, GRGS, and JPL) based on the noise decoupling problem (cf., Ferreira et al., 2016). In the RL05 monthly solutions, the degree-1 coefficients ( $C_{1,0}$ ,  $C_{1,1}$  and  $S_{1,1}$ ) were replaced by the results in Swenson et al. (2008), because GRACE gravity solutions do not provide those coefficients, which represent the changes in the geocenter due to mass redistribution in the Earth system. The inclusion of these coefficients would represent impacts on the amplitude of the annual and semi-annual GRACE-derived fields (Andam-Akorful et al., 2015). Because the GRACE-derived  $C_{2,0}$  coefficient as well as the coefficients  $C_{2,1}$ ,  $C_{2,2}$ ,  $S_{2,1}$  and  $S_{2,2}$  present relatively high uncertainties, they were replaced by the values derived from Satellite Laser Ranging (SLR) (Cheng and Tapley, 2004).

GRACE gravity fields at high-order coefficients exhibit a high level

of noise, which are known as “stripes” in the spatial domain (Swenson and Wahr, 2006). Therefore, in order to obtain coherent results, it is necessary to remove these stripes in post-processing by reducing correlated errors with minimal impact on the real signal. These correlations can be reduced by using either an empirical method based on a polynomial fit (Swenson and Wahr, 2006), or an *a priori* synthetic model of the observation geometry (Kusche, 2007). In this study, the convolution filter coefficients (Kusche, 2007), were applied to original GRACE-derived Stokes’s coefficients. Here, a weight factor  $a = 1 \times 10^{11}$  was adopted to smooth the monthly solutions called DDK5, and the level of smoothing approximately corresponded to a Gaussian smoothing radius of 240 km.

With respect to the GRACE uncertainty level (for the functional geoid height), it was estimated using the root-mean-square (rms) of the geoid heights over the Pacific Ocean as suggested in Chen et al. (2010). For a given month, the latitudes of  $56^\circ\text{S}$  and  $17^\circ\text{S}$  (the same latitude zone as the study region) and longitudes of  $180^\circ\text{W}$  and  $90^\circ\text{W}$  defined the geoid heights over a geographical region. This was necessary, as the calibrated errors of the spherical harmonics based on the UT-CSR solution up to d/o 96 were not available. While the estimation of GRACE errors could be improved by using the full covariance matrix (Jensen et al., 2013) and errors in the background models (Forootan et al., 2014), a comparison of the GRACE measurements with true observations would be more interesting for validation purposes (Ferreira et al., 2016). Nevertheless, the approach of Chen et al. (2010) provides an approximate measure of GRACE-derived geoid fields’ errors since the signal variations over the oceans is zero. Thus, any value different from zero reflects the error in GRACE measurements as well as the de-aliasing products (e.g. ocean model).

The mass variation near the surface can be expressed as time changes in geoid height ( $\dot{N}$ ) given by (Wahr et al., 1998):

$$\dot{N}(\theta, \lambda, t) = R \sum_{n=0}^{\infty} \sum_{m=0}^n [\delta\bar{C}_{nm}(t)\cos m\lambda + \delta\bar{S}_{nm}(t)\sin m\lambda] \bar{P}_{nm}(\cos\theta), \tag{4}$$

where  $\theta$ ,  $\lambda$ , and  $t$  are the co-latitude, longitude, and time, respectively,  $R$  is the mean radius of the Earth (6371 km),  $\delta\bar{C}_{nm}$  and  $\delta\bar{S}_{nm}$  are the residual Stokes coefficients obtained as the difference between the each monthly solution and the long term mean.  $\bar{P}_{nm}$  are the associated Legendre functions of degree  $n$  and order  $m$ . Eq. (4) was used for computing the geoid changes for the period of August 2002 to March 2016. Subsequently, 147 GRACE-derived geoid height monthly fields were resampled for exactly the middle of each month and the data of the missing months were linearly interpolated.

### 3.3. Estimation of earthquake signature in geodetic measurements

As mentioned in Section 1, the main goal of this work is to estimate

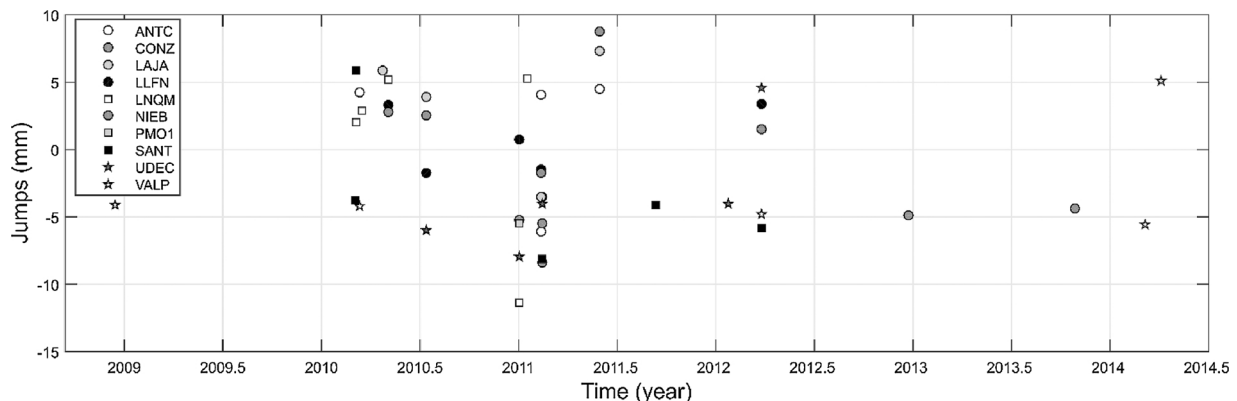


Fig. 2. Magnitude of the jumps produced by the main shallow minor earthquakes during the study period.

**Table 2**

Linear trend of the GIA, GNSS linear trend, co-seismic jump, annual ( $A_1$ ) and semi-annual ( $A_2$ ) amplitudes, parameters associated with post-seismic change, time from the earthquake occurrence ( $\Delta t$ ), and total post-seismic change.

Station	$\dot{h}_{GIA}$ [mm]	$\dot{h}$ [mm/year]	$\vartheta h_1$ [mm]	$A_1$ [mm]	$A_2$ [mm]	$a_1$ [mm]	$\Delta t$ [year]	$a_i \log(1 + \Delta t_i/T_i)$ [mm]
ANTC	0.4	2.37	-33.75	8.38	1.09	71.70	4.28	51.81
CONZ	0.3	-1.70	-49.43	4.72	0.43	-10.51	4.28	-7.60
LAJA	0.4	2.99	-31.95	9.03	0.21	33.71	4.08	23.80
LLFN	0.5	5.14	-11.25	3.88	2.57	13.20	4.03	9.26
LNQM	0.5	2.79	-12.96	6.86	1.19	36.78	3.83	25.15
NIEB	0.4	6.40	-21.65	5.68	0.75	-0.57	4.21	-0.41
PMO1	0.3	4.60	-4.59	6.07	1.92	5.68	3.75	3.84
SANT	0.3	4.0	-25.71	1.4	1.4	26.7	3.04	16.2
UDEC	0.3	-0.6	-340.24	5.2	0.7	15.5	4.22	11.2
VALP	0.3	1.8	-127.45	3.6	2.1	-3.6	4.28	-2.6

the deformation of CHVRF generated by co-seismic and post-seismic effects associated with the Maule Earthquake based on GNSS and GRACE observations. (All the quantities involved in the estimation of the co-seismic and post-seismic, i.e., ellipsoidal heights, orthometric heights, and geoidal undulations have been reduced to the zero-tide system). We considered the Maule earthquake, the hydrological loading and the GIA effects as predominant in the geodetic signal. Consequently, the modelling of these effects is necessary in calculating the impact of the Maule earthquake on orthometric heights. The hydrological loading can be considered from global hydrological models (e.g., Global Land Data Assimilation System – GLDAS). However, these models do not perform well in South America, principally due the lack of ground measurements (e.g., [Chen et al., 2009](#)).

Therefore, we assumed that the amplitudes and phases of the surface deformation due to hydrological loading came mainly from seasonal components, which generally repeat in consecutive years. (Noteworthy, signals encountered in hydrology, e.g., rainfall, have transient features, which lead to non-stationary processes). Then, we used a harmonic function with annual and semi-annual components in order to model the hydrological effects. (Time localized basis functions would have been preferred). We considered that the vertical deformation influenced by the GIA came from Earth's overall response to changes in ice-load after the last glacial period according a global model. It should be noted that several GIA models exist today, such as the ICE-3G ([Tushingham and Peltier, 1991](#)) and the ICE-4G ([Peltier, 1994](#)). However, we chose the recent model proposed by [Geruo et al. \(2013\)](#), as it represents the state-of-the-art in global estimation of the GIA effect. Its advantages include new results for compressible Earth, and it utilizes an elastic structure and viscosity profile with a continuously varying radius along the mantle, unlike older versions. For ellipsoidal and geoid heights, the uplift variations in the lithosphere ( $\dot{h}_{GIA}$ ) and linear trends in the geoid ( $\dot{N}_{GIA}$ ) filtered with a DDK5 were applied (compatible with GRACE filter scheme).

We considered the impact of the earthquake on the CHVRF benchmarks in the following way:

$$\begin{aligned}
 H(t) &= H(t_R) + \delta H \\
 \delta H &\approx \delta h_{GPS} - \delta N_{GRACE} \\
 &= (h_E + h_{GIA} + h_{HYD}) - (N_E + N_{GIA} + N_{HYD})
 \end{aligned} \quad (5)$$

Where  $t_R$  is a specific epoch and reference epoch respectively, and  $\delta H$ ,  $\delta h_{GPS}$ ,  $\delta N_{GRACE}$  indicates the temporal variations (linear and non-linear) associated with the effects of the earthquakes (E), glacial isostatic adjustment (GIA) and hydrological variations (HYD), on the orthometric, ellipsoidal and geoid heights respectively.

For modelling the trend of seasonal hydrological effects and (co-) post-seismic effects simultaneously on geodetic (GNSS and GRACE) time series, we used the following trajectory model ([Bevis and Brown, 2014](#)):

$$\begin{aligned}
 h(t) &= h_R + \dot{h}(t - t_R) + \sum_{j=1}^{n_j} \vartheta h_j \Omega(t - t_j) \\
 &+ \sum_{k=1}^2 [S_k \sin(\omega_k t) + C_k \cos(\omega_k t)] + \sum_{i=1}^{n_T} a_i \log(1 + \Delta t_i/T_i),
 \end{aligned} \quad (6)$$

where  $h_R$  is the ellipsoidal height in the reference epoch,  $\dot{h}$  is the velocity,  $t$  and  $t_R$  are the time in years and the reference time,  $\Omega$  is the Heaviside function,  $\vartheta h_j$  characterizes the jump which occurs at time  $t_j$  as an instantaneous displacement,  $S_k$  and  $C_k$  are the coefficients for computing the amplitude ( $A_k = \sqrt{S_k^2 + C_k^2}$ ) for each of the two frequencies (here annual and semi-annual waves),  $a_i$  is the magnitude of the exponential decay due of the post-seismic change in the period  $\Delta t$  in years since the earthquake occurred, and the decay time  $T$  was configured with default value  $T = 1$  year, reaching a good fit to the data. The total number of jumps and post-seismic effects are described by  $n_j$  and  $n_T$ , respectively. This study only modelled the post-seismic effect of the Maule earthquake, i.e.,  $n_T = 1$ . It is noteworthy that in the estimation of the parameters based on the GRACE time series, the term  $\Delta t_i$  is constant ( $\sim 6.0$  years from 2010 Maule Earthquake); this is because each series has the same length, which is not the case of the GNSS time series. Note that this model is insensitive to the effect of assigning a moderately erroneous value to the  $T$  parameter ([Bevis and Brown, 2014](#)). Our interest was in modelling the height motion of the station beyond understanding the physical causes. The parameters of the trajectory model were estimated by least squares adjustment.

#### 4. Results and discussion

The parameters of Eq. (6) were estimated by a least squares adjustment within a Gauss Markov Model. It is possible to see from [Table 2](#) that, for almost all GNSS stations, remarkable hydrological and (co-) post-seismic effects are present in the series. The hydrological effects associated to annual and semi-annual amplitudes reached  $\sim 9$  mm and  $\sim 3$  mm at LAJA and LLFN stations, respectively. The maximum co- and post-seismic effects reached values of approximately  $-340$  mm and  $52$  mm at the UDEC and ANTC stations, respectively (see [Fig. 3](#)). In addition, LAJA and LNQM stations present significant post-seismic deformation ( $> 20$  mm). The rest of the stations did not reveal considerable exponential viscoelastic relaxation after the earthquake ( $< 20$  mm).

The result of the logarithmic transient term associated to post-seismic change during at the period observed in the GNSS stations showed heterogeneous results. For the ANTC, LAJA and LNQM stations located in the Andes Mountains, the values of the total post-seismic change revealed uplifts of about  $24$  mm to  $52$  mm, while CONZ and VALP stations located on the coast, showed subsidences of approximately  $-8$  mm to  $-3$  mm ([Table 2](#)).

Regarding the analysis of the geoid time series, the co-seismic effect caused a subsidence in the geoid that reached  $-3.3$  mm in the SANT station. The hydrological contribution reached a maximum amplitude

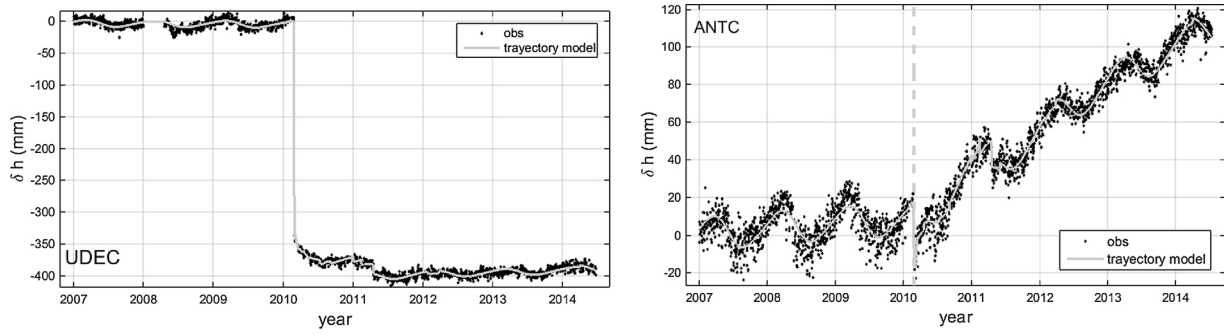


Fig. 3. Time series for the GNSS stations of UDEC and ANTC, which show the largest jump and post-seismic effect in ellipsoidal heights.

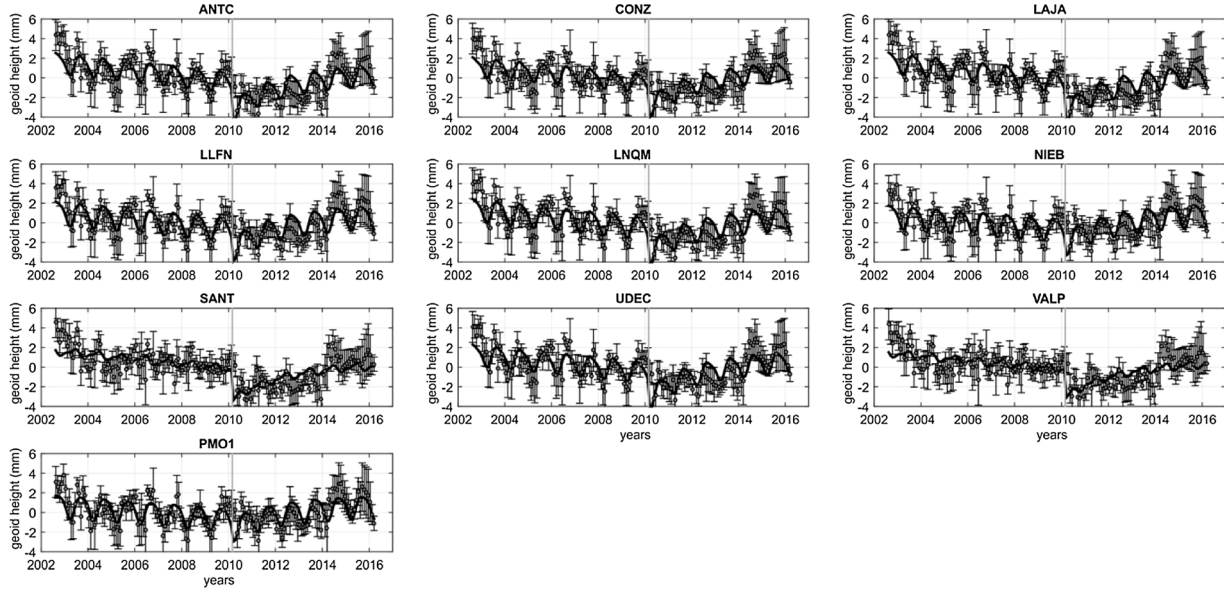


Fig. 4. Time series of the geoid heights for all stations considered in this study. The black line represents the trajectory model (Eq. (6)) and vertical grey line represent the Maule Earthquake epoch. The error bars represent the GRACE errors estimated as the root-mean-square (rms) of the geoid heights over the region 90°W–180°W and 17°S–56°S.

Table 3  
Parameters to geoid time series and GIA effect.

Station	$\dot{N}_{GIA}$ [mm/year]	$\dot{N}$ [mm/year]	$\vartheta N_1$ [mm]	$A_1$ [mm]	$A_2$ [mm]	$a_1$ [mm]	$a_1 \log(1 + \Delta t_i/T_i)$ [mm]
ANTC	0.11	-0.26	-3.12	0.99	0.23	2.77	2.35
CONZ	0.10	-0.23	-2.61	0.89	0.25	2.66	2.25
LAJA	0.11	-0.27	-3.16	1.00	0.22	2.78	2.35
LLFN	0.12	-0.22	-2.11	1.15	0.26	2.41	2.04
LNQM	0.12	-0.25	-2.66	1.11	0.24	2.63	2.23
NIEB	0.12	-0.18	-1.47	1.12	0.27	2.11	1.79
PMO1	0.13	-0.19	-1.10	1.14	0.25	1.81	1.53
SANT	0.10	-0.24	-3.33	0.33	0.15	2.59	2.19
UDEC	0.11	-0.24	-2.73	1.01	0.25	2.67	2.26
VALP	0.01	-0.22	-2.98	0.30	0.16	2.49	2.11

of ~1.2 mm and 0.3 mm in terms of annual and semi-annual periods at the LLFN and NIEB stations, respectively (see Fig. 4 and Table 3).

The GIA uplift effects showed values of approximately 0.1 mm/year. The geoid post-seismic rate reached values of about 2.4 mm (see Table 3). Furthermore, no significant correlation can be observed with respect to the post-seismic values found in the GNSS time series (correlation coefficient 0.49 in  $a_1$  parameter). Possible reasons are non-regular seasonal changes, large inter-annual variations, difficulty in separating the hydrological signal, the presence of other processes such as afterslip on the plate interface and viscoelastic relaxation, and the increase of errors in the GRACE observations over time (Fig. 4).

Nevertheless, one of the reasons why the signal from the Maule

earthquake (shallow Earthquake, depth ~30 km) over GRACE observations is not as intense as that reflected on the Earth’s surface by GNSS measurements seems to be due to the fact that a large part of the earthquake signal is located on the surface, and at short wavelengths (> degree and order 96) where GRACE observations are not sensitive. Examples of earthquakes of similar magnitude (e.g., Japan Tohoku-Oki earthquake of 9.0 Mw), explored by GOCE observations with better spatial resolution have shown geoid height variations between 0.8 to -1.2 cm (Fuchs et al., 2013).

On the other hand, we compared the velocities from VEMOS2015 with those estimated herein, and obtained an rms of 8.2 mm/year. We attributed these differences mainly to correction models, fiducial

**Table 4**  
Co-seismic jump in mm for all stations.

Station	$\vartheta h$	$\vartheta N$	$\vartheta H$
ANTC	-33.75	-3.12	-30.63
CONZ	-49.43	-2.61	-46.82
LAJA	-31.95	-3.16	-28.79
LLFN	-11.25	-2.11	-9.14
LNQM	-12.96	-2.66	-10.30
NIEB	-21.65	-1.47	-20.18
PMO1	-4.59	-1.10	-3.49
SANT	-25.71	-3.33	-22.38
UDEC	-340.24	-2.73	-337.51
VALP	-127.45	-2.98	-124.47

stations used in the network adjustment, models used in the velocity estimation and the data periods used. For example, [Sánchez and Drewes \(2016\)](#) have reported that the period associated with post-seismic signal was removed from the weekly normal equations, and only constant velocities are estimated for constructing the VEMOS2015. Due to the heterogeneous distribution, a low number of continuous GNSS stations and the low adherence of velocities estimated with those of the VEMOS2015 models, it becomes complicated to fill the velocity term in the trajectory model (Eq. (6)) in the study region.

The co-seismic jump on the ellipsoidal heights and the geoid height was calculated by (6), and the results are presented in [Table 4](#).

The co-seismic effects on the ellipsoidal heights, which are generally implied to quantify uplift/subsidence, show maximum and minimum subsidence values of approximately  $-34$  cm and  $-0.3$  cm at the stations of UDEC and PMO1, respectively (see [Table 5](#)).

To measure the correlation between the deformation occurring at the Earth's surface and at the geoid, we estimated the correlation coefficient with the GNSS and GRACE time series. Before estimating the correlation, we harmonized the GNSS time series, i.e., by applying a low pass filter using a one month window average and by removing the effects caused by other minor earthquakes as well as jumps by the antenna change, assuming that these are not present in the signal inverted from GRACE measurements. Overall, the results revealed a low correlation with the highest value of about 0.7 for the VALP station and the lowest of 0.0 for the NIEB station. We believe that most of the surface variations occur in a time and space domain of short wavelength frequencies, which are not reached by GRACE based modelling (see [Table 5](#)).

Co-seismic effects on orthometric heights ( $\vartheta H(k)$ ) were calculated using the following expression (see [Table 4](#) and [Fig. 5](#)):

$$\vartheta H(k) = \vartheta h(k) - \vartheta N(k) \quad (7)$$

where  $\vartheta h(k)$  and  $\vartheta N(k)$  are the co-seismic effect in ellipsoidal heights and geoid at the  $k$ -th station, respectively. It should be noted that the co-seismic effect on the ellipsoidal height was calculated from the equation (6) for the ten continuous GNSS stations and calculated as the difference between the heights estimated before and after the earthquake in the case of observations from GNSS measurement campaigns.

**Table 5**  
Correlation coefficients ( $\rho$ ) between  $\dot{h}$  and  $\dot{N}$ .

Station	$\rho$	Station	$\rho$
ANTC	-0.3	NIEB	0.0
CONZ	0.3	PMO1	-0.1
LAJA	-0.3	SANT	-0.6
LLFN	-0.1	UDEC	-0.3
LNQM	-0.5	VALP	0.7

The stations located between  $-38^\circ < \varphi < -34^\circ$  experienced a higher co-seismic subsidence from 20 cm, up to 60 cm (see [Fig. 5](#)). The post seismic effect was calculated from the ten continuous GNSS stations. It should be noted that a short post seismic effect (2010–2015) was estimated in this study. This could remain for years, but with a rate of change lower than that of our analysis period.

We observed that, after removal of the hydrologic effect on GNSS and GRACE time series, the time series of orthometric heights did not present significant periodic components.

The CHVRF design is based on a set of lines of leveling densified from west to east direction and it is based on many segments with each of them is associated with a specific tide gauge, without connection among them. Thus, considering the characteristics of the CHVRF and the co-seismic deformation, which are also predominantly distributed at west-east direction, the co- and post-seismic effects due to the Maule Earthquake on CHVRF translates only in modelling this effect without considering the influence of the systematic errors in the network. These systematic errors are mainly due to the constrained adjustment considering each tide gauge; each tide gauge materializes a different equipotential surface of zero height (local geoids).

According to our results, the CHVRF should introduce kinematic aspects in their maintenance, such as using a trajectory model similar to the one presented here (Eq. (6)). Exchange rates experienced in the ellipsoidal heights from different geodynamic phenomena must be considered for determining orthometric heights, with the purpose of predicting heights and maintaining a modern multi-purpose heights system. On the other hand, the geoid is sensitive to mass changes such as those caused by the Maule Earthquake, though deformations reach only a couple of millimeters. As GRACE solutions are limited in terms of spectral/spatial resolution (d/o 96 equivalent to half-wavelength of about  $\sim 200$  km), ground- and air-borne gravity measurements could improve the estimation of geoid height changes. Thus, the majority of the signal contained in the short wavelengths of Earth's gravity field would be better recovered. In this sense, the results can be considered preliminary and must be interpreted with caution. We estimate that it is only possible to reach variations of the geoid that could influence the Vertical Reference Frame within the considered region by following longer periods ( $> 5$  years) than those used in the present analysis. In the period considered here, we can ponder that most of orthometric height variations can be explained by the ellipsoidal height changes observed with GNSS.

## 5. Conclusion and future prospects

In this study, we have presented the first estimation of the impact of the 2010 Maule Earthquake deformation on the CHVRF, considering an indirect strategy based on GNSS and GRACE observations, and a trajectory model. The earthquake generated an important co-seismic subsidence as observed at almost all stations considered in this study, which must be considered when updating the heights associated with the segments of CHVRF in the study region.

It was observed that the deformation signal associated with the segments of the CHVRF due to the earthquake was almost completely recovered ( $\sim 85\%$ ) by the variations in the ellipsoidal heights derived from GNSS. However, the variations experienced in the geoid due to earthquakes, GIA and hydrologic effects, should be considered in long periods ( $> 5$  years) for the purpose of achieving the maintenance requirements of the modern vertical geodetic network with a relative accuracy of the order of 3 ppm.

The co-seismic and post-seismic effects associated with the Maule Earthquake showed predominant discontinuity characteristics in the east-west direction near the epicenter. It should be noted that the behavior of the stations located farther from the epicenter do not necessarily reveal the Maule Earthquake signal, as they may contain superposing effects from other phenomena.

Our results show the possibility of an indirect temporal analysis of

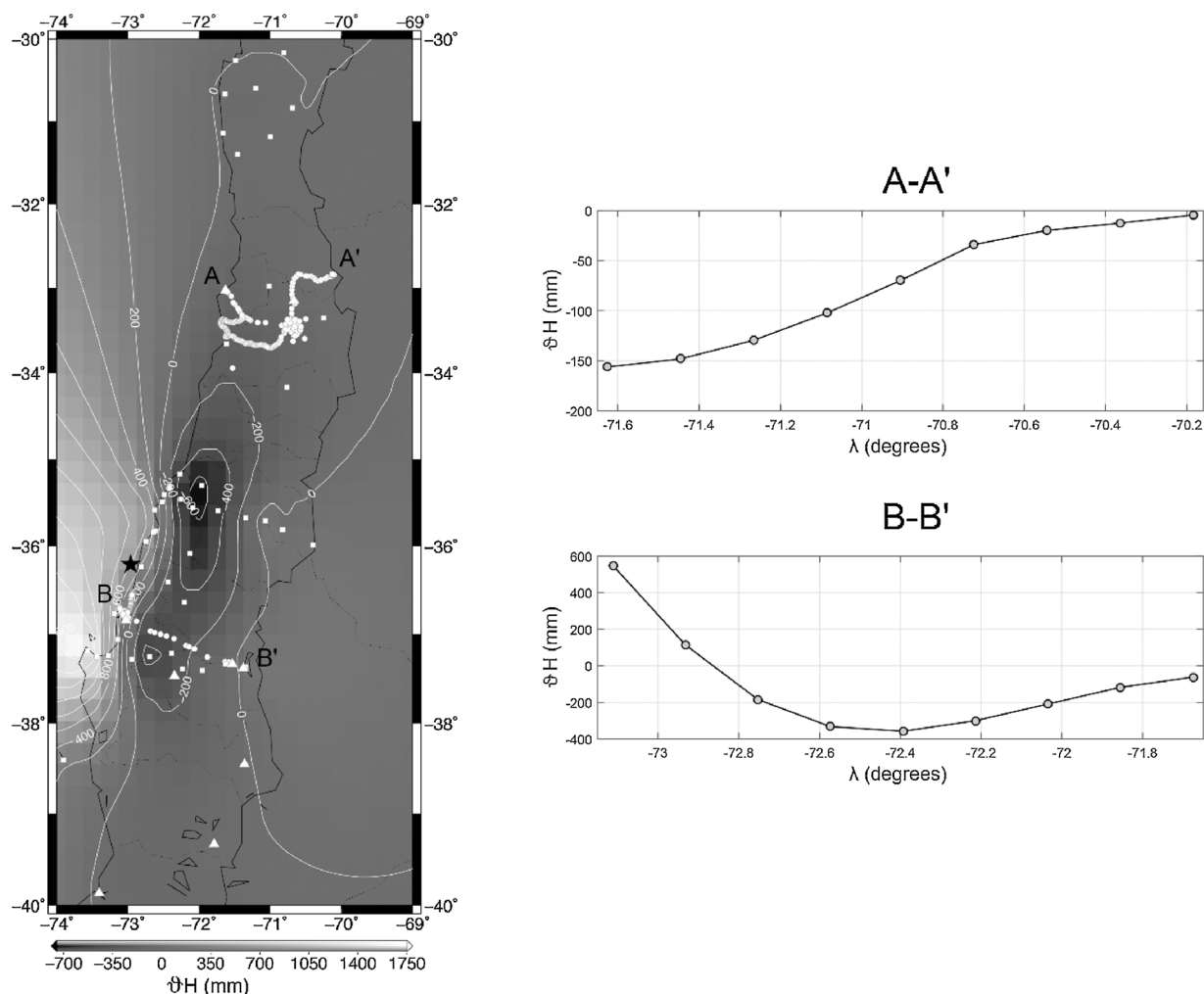


Fig. 5. Spatial distribution of co-seismic effects on orthometric heights due to the Maule earthquake. Left panel: Contours of co-seismic effect, GNSS stations and leveling lines. Right panel: profiles of the co-seismic deformation around the leveling lines most affected by the earthquake.

orthometric heights realized through the combination of velocities, periodic components, jumps and post-seismic relaxation based on GNSS and GRACE observations integrated into a trajectory model with moderate spatial resolution. The methodology presented here could be used to update a height system, especially in regions with a predominant seismic activity and hydrological signal.

We recommend a validation study of the proposed methodology, based on re-leveling some of the leveled lines in the study region in association with gravity for obtaining the effects in the geopotential space.

Regarding the poor and heterogeneous distribution of GNSS stations to model the effects associated with short wavelengths, we are studying the possibility of recovering temporal deformation models through the combination and interpolation of GNSS (2D + 1D) and InSAR (1D) observations and a jointly inversion with GRACE observations over the study region.

Finally, according to the estimation and analysis of the space-time deformations of the segments of the CHVRF presented here, we advise taking precautions when using the data, because the introduced distortions of deformation of the network could be greater than the tolerances accepted in some applications, such as civil engineering projects.

**Acknowledgements**

Author Henry Montecino would like to thank the PhD scholarship

granted by the University of Concepción (UdeC). The author Silvio de Freitas thanks CNPq (Grant process N. 306936/2015-1). Vagner Ferreira acknowledges the partial support provided by the National Natural Science Foundation of China through a grant No. 42574001. The authors thank the CSR, GFZ and JPL processing centers for providing monthly solutions of the gravity field, the Earth Science Division of NASA for the distribution of GLDAS, the CAP projects, IGS, and BKG and the Universidad de Chile for providing the GPS observations used here. We thank Professor Irina Artemieva (Editor-in-Chief) and the two anonymous reviewers for their constructive comments that helped us to improve the quality of this manuscript.

**Appendix A. Supplementary data**

Supplementary data associated with this article can be found, in the online version, at <http://dx.doi.org/10.1016/j.jog.2017.07.006>.

**References**

Andam-Akorful, S.A., Ferreira, V.G., Awange, J.L., Forootan, E., He, X.F., 2015. Multi-model and multi-sensor estimations of evapotranspiration over the Volta Basin, West Africa. *Int. J. Climatol.* 35, 3132–3145. <http://dx.doi.org/10.1002/joc.4198>.  
 Becker, J.J., Sandwell, D.T., Smith, W.H.F., Braud, J., Binder, B., Depner, J., Fabre, D., Factor, J., Ingalls, S., Kim, S.-H., Ladner, R., Marks, K., Nelson, S., Pharaoh, A., Trimmer, R., Von Rosenberg, J., Wallace, G., Weatherall, P., 2009. Global bathymetry and elevation data at 30 arc seconds resolution: SRTM30\_PLUS. *Mar. Geod.* 32, 355–371. <http://dx.doi.org/10.1080/01490410903297766>.  
 Bettadpur, S., 2012. UTCSR Level-2 processing standards document for Level-2 product

- release 0005, GRACE 327–742, Rev. 4.0.
- Bevis, M., Brown, A., 2014. Trajectory models and reference frames for crustal motion geodesy. *J. Geod.* 88, 283–311. <http://dx.doi.org/10.1007/s00190-013-0685-5>.
- Boehm, J., Niell, A., Tregoning, P., Schuh, H., 2006. Global Mapping Function (GMF): a new empirical mapping function based on numerical weather model data. *Geophys. Res. Lett.* 33. <http://dx.doi.org/10.1029/2005gl025546>.
- Bruinsma, S., Lemoine, J.-M., Biancale, R., Valès, N., 2010. CNES/GRGS 10-day gravity field models (release 2) and their evaluation. *Adv. Sp. Res.* 45, 587–601. <http://dx.doi.org/10.1016/j.asr.2009.10.012>.
- Chen, J.L., Wilson, C.R., Tapley, B.D., Yang, Z.L., Niu, G.Y., 2009. 2005 drought event in the Amazon River basin as measured by GRACE and estimated by climate models. *J. Geophys. Res. Solid Earth* 114. <http://dx.doi.org/10.1029/2008jb006056>.
- Chen, J.L., Wilson, C.R., Tapley, B.D., 2010. The 2009 exceptional Amazon flood and interannual terrestrial water storage change observed by GRACE. *Water Resour. Res.* 46, 1–10. <http://dx.doi.org/10.1029/2010WR009383>.
- Cheng, M., Tapley, B.D., 2004. Variations in the Earth's oblateness during the past 28 years. *J. Geophys. Res.* 109, B09402. <http://dx.doi.org/10.1029/2004JB003028>.
- De Linage, C., Rivera, L., Hinderer, J., Boy, J.P., Rogister, Y., Lambotte, S., Biancale, R., 2009. Separation of coseismic and postseismic gravity changes for the 2004 Sumatra – Andaman earthquake from 4.6 yr of GRACE observations and modelling of the coseismic change by normal-modes summation. *Geophys. J. Int.* 176, 695–714. <http://dx.doi.org/10.1111/j.1365-246X.2008.04025.x>.
- Drewes, H., Heidbach, O., 2012. The 2009 horizontal velocity field for South America and the Caribbean. In: Kenyon, S., Pacino, M.C., Marti, U. (Eds.), *Geodesy for Planet Earth SE – 81*, International Association of Geodesy Symposia. Springer, Berlin Heidelberg, pp. 657–664. [http://dx.doi.org/10.1007/978-3-642-20338-1\\_81](http://dx.doi.org/10.1007/978-3-642-20338-1_81).
- Du, Y., Wang, Z., Yang, S., An, J., Liu, Q., Che, G., 2013. Co-seismic deformation derived from GPS observations during april 20th, 2013 Lushan earthquake, Sichuan, China. *Earthq. Sci.* 26, 153–160. <http://dx.doi.org/10.1007/s11589-013-0014-3>.
- Ferreira, V.G., Montecino, H.D.C., Yakubu, C.I., Heck, B., 2016. Uncertainties of the Gravity Recovery and Climate Experiment time-variable gravity-field solutions based on three-cornered hat method. *J. Appl. Remote Sens.* 10, 015015. <http://dx.doi.org/10.1117/1.JRS.10.015015>.
- Forootan, E., Didova, O., Schumacher, M., Kusche, J., Elsaka, B., 2014. Comparisons of atmospheric mass variations derived from ECMWF reanalysis and operational fields, over 2003–2011. *J. Geod.* 88, 503–514. <http://dx.doi.org/10.1007/s00190-014-0696-x>.
- Fuchs, M.J., Bouman, J., Broerse, T., Visser, P., Vermeersen, B., 2013. Observing co-seismic gravity change from the Japan Tohoku-Oki 2011 earthquake with GOCE gravity gradiometry. *J. Geophys. Res. Solid Earth* 118, 5712–5721. <http://dx.doi.org/10.1002/jgrb.50381>.
- Geruo, A., Wahr, J., Zhong, S., 2013. Computations of the viscoelastic response of a 3-D compressible earth to surface loading: an application to glacial isostatic adjustment in Antarctica and Canada. *Geophys. J. Int.* 192, 557–572. <http://dx.doi.org/10.1093/gji/ggs030>.
- Heki, K., Matsuo, K., 2010. Coseismic gravity changes of the 2010 earthquake in central Chile from satellite gravimetry. *Geophys. Res. Lett.* 37. <http://dx.doi.org/10.1029/2010gl045335>.
- Hofmann-Wellenhof, B., Moritz, H., 2005. *Physical geodesy*. Phys. Geod., 1st ed. Springer-Verlag Wien, Vienna, pp. XVII, 403. <http://dx.doi.org/10.1007/b139113>.
- Ihde, J., Barzaghi, R., Marti, U., Sánchez, L., Sideris, M., Drewes, H., Foerste, C., Gruber, T., Liebsch, G., Pail, R., 2015. Report of the ad hoc group on an International Height Reference System (IHRs).
- Jacob, T., Wahr, J., Gross, R., Swenson, S.A.G., 2012. Estimating geoid height change in North America: past, present and future. *J. Geod.* 86, 337–358. <http://dx.doi.org/10.1007/s00190-011-0522-7>.
- Jensen, L., Rietbroek, R., Kusche, J., 2013. Land water contribution to sea level from GRACE and Jason-1 measurements. *J. Geophys. Res. Oceans* 118, 212–226. <http://dx.doi.org/10.1002/jgrc.20058>.
- Kusche, J., 2007. Approximate decorrelation and non-isotropic smoothing of time-variable GRACE-type gravity field models. *J. Geod.* 81, 733–749. <http://dx.doi.org/10.1007/s00190-007-0143-3>.
- Li, J., Shen, W., 2012. GRACE detection of the medium- to far-field coseismic gravity changes caused by the 2004 MW9.3 Sumatra-andaman earthquake. *Earthq. Sci.* 25, 235–240. <http://dx.doi.org/10.1007/s11589-012-0849-z>.
- Lin, Y.N.N., Sladen, A., Ortega-Culaciati, F., Simons, M., Avouac, J.P., Fielding, E.J., Brooks, B. a., Bevis, M., Genrich, J., Rietbrock, A., Vigny, C., Smalley, R., Socquet, A., 2013. Coseismic and postseismic slip associated with the 2010 Maule Earthquake, Chile: characterizing the Arauco Peninsula barrier effect. *J. Geophys. Res. Solid Earth* 118, 3142–3159. <http://dx.doi.org/10.1002/jgrb.50207>.
- Maturana, R., Barriga, R., 2002. The vertical geodetic network in Chile. *Vertical Reference Systems*. Springer, pp. 23–26.
- Moreno, M., Melnick, D., Rosenau, M., Bolte, J., Klotz, J., Echter, H., Baez, J., Bataille, K., Chen, J., Bevis, M., Hase, H., Oncken, O., 2011. Heterogeneous plate locking in the South-Central Chile subduction zone: building up the next great earthquake. *Earth Planet. Sci. Lett.* 305, 413–424. <http://dx.doi.org/10.1016/j.epsl.2011.03.025>.
- Panet, I., Mikhailov, V., Diament, M., Pollitz, F., King, G., de Viron, O., Holschneider, M., Biancale, R., Lemoine, J.M., 2007. Coseismic and post-seismic signatures of the Sumatra 2004 December and 2005 March earthquakes in GRACE satellite gravity. *Geophys. J. Int.* 171, 177–190. <http://dx.doi.org/10.1111/j.1365-246X.2007.03525.x>.
- Peltier, W.R., 1994. Ice age paleotopography. *Science* 265, 195–201. <http://dx.doi.org/10.1126/science.265.5169.195>.
- Pollitz, F.F., Brooks, B., Tong, X., Bevis, M.G., Foster, J.H., Bürgmann, R., Smalley, R., Vigny, C., Socquet, A., Ruegg, J.C., 2011. Coseismic slip distribution of the february 27, 2010 mw 8.8 Maule, Chile earthquake. *Geophys. Res. Lett.* 38.
- Rangelova, E., Fotopoulos, G., Sideris, M.G., 2010. Implementing a dynamic geoid as a vertical datum for orthometric heights in Canada. *International Association of Geodesy Symposia*. pp. 295–302. [http://dx.doi.org/10.1007/978-3-642-10634-7\\_38](http://dx.doi.org/10.1007/978-3-642-10634-7_38).
- Rangelova, E., Van Der Wal, W., Sideris, M.G., 2012. How significant is the dynamic component of the North American Vertical Datum? *J. Geod. Sci.* 2, 281–289. <http://dx.doi.org/10.2478/v10156-012-0005-7>.
- Rivas, L., 2010. Consecuencias del terremoto del 27 de febrero de 2010 en la red geodésica nacional y la cartografía. *Meml. del Ejército Chile. D. Comun. del ejército* 485, 136–149.
- Sánchez, L., Drewes, H., 2015. Post-seismic Crustal Deformations After the 2010 Earthquakes in Latin America. *IUGG 2015*.
- Sánchez, L., Drewes, H., 2016. Crustal deformation and surface kinematics after the 2010 earthquakes in Latin America. *J. Geod.* 102, 1–23. <http://dx.doi.org/10.1016/j.jog.2016.06.005>.
- Schmid, R., Steigenberger, P., Gendt, G., Ge, M., Rothacher, M., 2007. Generation of a consistent absolute phase-center correction model for GPS receiver and satellite antennas. *J. Geod.* 81, 781–798. <http://dx.doi.org/10.1007/s00190-007-0148-y>.
- Sun, W., 2014. Recent advances of computing coseismic deformations in theory and applications. *Earthq. Sci.* 27, 217–227. <http://dx.doi.org/10.1007/s11589-014-0077-9>.
- Swenson, S., Wahr, J., 2006. Post-processing removal of correlated errors in GRACE data. *Geophys. Res. Lett.* 33. <http://dx.doi.org/10.1029/2005gl025285>.
- Swenson, S., Chambers, D., Wahr, J., 2008. Estimating geocenter variations from a combination of GRACE and ocean model output. *J. Geophys. Res. Solid Earth* 113. <http://dx.doi.org/10.1029/2007JB005338>.
- Tanaka, Y., Heki, K., 2014. Long-and short-term postseismic gravity changes of megathrust earthquakes from satellite gravimetry. *Geophys. Res. Lett.* 41, 5451–5456.
- Tapley, B.D., Bettadpur, S., Watkins, M., Reigber, C., 2004. The gravity recovery and climate experiment: mission overview and early results. *Geophys. Res. Lett.* 31. <http://dx.doi.org/10.1029/2004gl019920>.
- Tushingham, A.M., Peltier, W.R., 1991. Ice-3G: A new global model of Late Pleistocene deglaciation based upon geophysical predictions of post-glacial relative sea level change. *J. Geophys. Res.* 96, 4497–4523. <http://dx.doi.org/10.1029/90JB01583>.
- Vigny, C., Socquet, A., Peyrat, S., Ruegg, J.-C., Métois, M., Madariaga, R., Morvan, S., Lancieri, M., Lacassin, R., Campos, J., Carrizo, D., Bejar-Pizarro, M., Barrientos, S., Armijo, R., Aranda, C., Valderas-Bermejo, M.-C., Ortega, I., Bondoux, F., Baize, S., Lyon-Caen, H., Pavez, A., Vilotte, J.P., Bevis, M., Brooks, B., Smalley, R., Parra, H., Baez, J.-C., Blanco, M., Cimbaro, S., Kendrick, E., 2011. The 2010 mw 8.8 Maule megathrust earthquake of central Chile, monitored by GPS. *Science* 332, 1417–1421. <http://dx.doi.org/10.1126/science.1204132>.
- Wahr, J., Molenaar, M., Bryan, F., 1998. Time variability of the Earth's gravity field: hydrological and oceanic effects and their possible detection using GRACE. *J. Geophys. Res.* 103, 30205–30229. <http://dx.doi.org/10.1029/98JB02844>.